# Modelling Aquifer Thermal Energy Storage (ATES) System with Buoyancy Flow

Markus Gillner<sup>1</sup> Arne Speerforck<sup>1</sup>

<sup>1</sup>Hamburg University of Technology, am Schwarzenberg-Campus 1, Hamburg, Germany, Institute of Engineering Thermodynamics, {markus.gillner,arne.speerforck}@tuhh.de

#### **Abstract**

Aquifer Thermal Energy Storages (ATES) as long-term storages have a strong potential to address the seasonal discrepancy of supply and demand of thermal energy. The operation of high-temperature ATES (HT-ATES) and their integration into district heating systems are the subject of current research projects. Buoyancy plays an important role in determining how HT-ATES performs. The target of this paper is to present a system model in Modelica that takes these buoyancy effects into account. The validation with experimental data and numerical simulations shows that the system model represents the buoyancy effects well. A sensitivity analysis underlines the importance of optimizing the grid structure and shows that a high resolution in the aquifer is necessary, especially in the vertical direction. Finally, a 10-year simulation shows the deviation of the heat recovery factor, i.e. the ratio of the amount of heat extracted to the amount of heat injected, between a model with and without buoyancy effects.

Keywords: High Temperature Aquifer Thermal Energy Storage, ATES, Buoyancy, System Model, TransiEnt Library

### 1 Introduction

In 2023, only 17% of Germany's final energy consumption in the heating sector was produced from renewable sources (Umweltbundesamt 2024). One of the major challenges transforming the heating transition is the seasonal offset between the supply of sustainable heat and demand. Aquifer thermal energy storage (ATES) is one of the most promising seasonal storage systems due to its high storage capacity, efficiency and small above-ground footprint (Guelpa and Verda 2019). The principle of ATES is based on two wells (doublets) drilled into water-bearing soil layers, called aquifer. Thermal water is extracted from one well (cold or compensation well), heated and injected into the second well (hot well). During the heating period, the heated thermal water is pumped up from the hot well, the heat is extracted via heat exchangers and returned to the second well.

A distinction is made between low-temperature ( $< 50^{\circ}\text{C}$ ) and high-temperature ( $\geq 50^{\circ}\text{C}$ ) aquifer storage, depending on the temperature of the thermal water to be stored. Due to the low temperature level, LT-ATES

also serve as cold storage for the summer. While LT-ATES are widely used, only 5 HT-ATES are in operation worldwide (Fleuchaus 2020). Some have been closed after years of operation (e.g. Utrecht University, Hooge Burch in Zwammerdam and Neubrandenburg). In Neubrandenburg and Hooge Burch, Zwammerdam this was due to uneconomic operation due to fluctuating heat demand and supply (Fleuchaus et al. 2021; Drijver, Bakema, and Oerlemans 2019). The ATES at the University of Utrecht closed due to problems in the well and a discrepancy between the required temperature level and the temperature supplied from the aquifer storage (Drijver, Bakema, and Oerlemans 2019). This means that the interaction between the aquifer storage and its surroundings, be it individual buildings or district heating systems with their fluctuating heat demand and supply, requires further research.

New HT-ATES projects such as the Living Lab "GeoSpeicher Berlin" (Federal Ministry for Economic Affairs and Climate Action 2024) and "PUSH-IT" (Push it 2024) are building HT-ATES systems for integration into district heating systems, and projects such as "ATES Vienna" (Forschungsinitiative Green Energy Lab 2022) and "OptInAquiFer" (Hamburg Insitut 2022) are investigating the integration of HT-ATES into district heating systems. Köhler et al. (2025) from the OptInAquiFer project have identified a great potential for seasonal thermal energy storage in district heating systems, for which detailed models for the realisation of efficient storage systems are needed in order to be able to investigate the grid-side challenges in advance.

The most commonly used computer codes for the simulation of underground aquifers are complex CFD-based codes such as FEFLOW (DHI-WASY GmbH 2012), OpenGeoSys (Kolditz et al. 2012), MODFLOW (Langevin et al. 2017), HSTWin-2D (Kipp 1987) etc. These programs can represent complex geometries and take into account physical effects such as chemical reactions and groundwater flow in addition to heat and mass transport, but are only marginally suitable for system analysis. The simulation of aquifer storage in systems can only be represented with these programs using complex co-simulations. System level modelling platforms such as TRNSYS and Modelica are suitable for modelling the interaction of aquifer storage systems with buildings and district heating. For both modelling platforms, ATES

models already exist. The TRNAST (Schmidt 2005) model for TRNSYS allows the simulation of an aquifer storage system whose wells are thermally and hydraulically separated from each other. Heat transport is radial and vertical, while mass transport is radial only. The model of Maccarini et al. (2023) in the Modelica library IBPSA is a low-order model that is designed for fast numerical calculation and therefore only transports heat and mass radially. Both models neglect buoyancy flow due to larger temperature differences in the aquifer.

Various literature and studies have shown that buoyancy flow can have a significant impact on the efficiency of ATES systems (Buscheck, Doughty, and Tsang 1983; Gao et al. 2024; Beernink et al. 2024; Heldt, Beyer, and Bauer 2024). Gao et al. (2024) have shown with a non-dimensional approach that the design of the temperature profile in the aquifer can be classified into three different regimes: Conduction dominated, buoyancy dominated and a transition regime. Nield and Bejan (2013) gives the critical Rayleigh-Darcy number above which buoyancy can no longer be neglected as

$$Ra_{critical} = \frac{g\rho_{\rm f}^2 c_{p,a} \beta \Delta T K L}{\mu \lambda} = 4\pi^2, \qquad (1)$$

with  $\beta$  as the thermal expansion coefficient, g as the gravitational acceleration,  $\rho_{\rm f}$  as the density,  $c_{p,a}$  as the specific heat capacity of the aquifer, K as the permeability, L as the characteristic length (here: height of aquifer),  $\mu$ as the dynamic viscosity and  $\lambda$  as the thermal diffusivity. This means that even at low permeabilities (e.g. 0.1 Darcy) the temperature difference between injected and existing thermal water must not exceed 40°C. This is almost always exceeded for high-temperature storage tanks. In addition to 2D heat transport, the ATES model presented here also takes buoyancy flow into account. In section 2 the mathematical and numerical model is described and validated against experimental and numerical data in section 3. section 4 presents an example for a 10 Years simulation of an ATES and in section 5 the main results are summarized. The entire model is to be added to the TransiEnt library (Gillner et al. 2025).

## 2 Method

The purpose of the model is to simulate the thermohydraulic behaviour of an ATES system for high and low temperature injection. The model should then be suitable for integration into larger system levels.

#### 2.1 Modeling approach

The following assumptions are made in the model:

- The aquifer is homogenous and isotropic, so a 2D cylindrical representation is sufficient.
- A local thermal equilibrium between the fluid and the solid phase is assumed.

- Regional groundwater flow is neglected.
- Thermal interference between hot and cold well is neglected.
- The fluid in the aquifer is assumed to be pure water.
- The porosity, the permeability, the height of the layers and the material properties of the solid phase are constant.
- Radiative effects, viscous dissipation and work done by pressure changes are neglected in the energy equation.
- The well screen fully penetrates the aquifer.
- The aquifer is confined by impermeable layers above and below.

The last two assumptions depend on the modeling. They can be adjusted with little effort.

To describe convection and conduction in the aquifer, the model is based on the three governing equations for mass, momentum and energy conservation. The mass conservation equation is given by

$$\phi \cdot \frac{\partial \rho_{f}}{\partial t} + \nabla \cdot (\rho_{f} \cdot \mathbf{v}) = 0, \tag{2}$$

where  $\phi$  is the porosity,  $\rho_f$  is the fluid density and  $\mathbf{v}$  is the seepage velocity or also called Darcy flux given as  $\mathrm{m}^3\,\mathrm{m}^{-2}$ . The subscript f refers to fluid. The momentum conservation equation for porous medium considering laminar flow is given by

$$\mathbf{v} = -\frac{\mathbf{K}}{\mu} (\nabla p - \rho_f \mathbf{g}), \tag{3}$$

where **K** is the permeability tensor,  $\mu$  is the dynamic viscosity, p is the pressure, and **g** is the gravitational acceleration vector. The energy conservation equation in the aquifer is given by

$$(\rho c_{\mathbf{p}})_{\mathbf{a}} \frac{\partial T}{\partial t} + (\rho c_{\mathbf{p}})_{\mathbf{f}} \mathbf{v} \cdot \nabla T = k_{\mathbf{a}} \cdot \nabla \cdot (\nabla T),$$
 (4)

where c is the heat capacity, T is the temperature, k is the thermal conductivity, and the subscript a represents the coupled material values of the liquid and solid phase. As the model is assumed to be in thermal equilibrium, heat conduction is parallel in both phases. For an effective thermal conductivity, density and heat capacity, the weighted arithmetic mean is used as follows:

$$k_{\rm a} = (1 - \phi) k_{\rm s} + \phi k_{\rm f},$$
 (5)

$$\rho_{\rm a} = (1 - \phi) \rho_{\rm s} + \phi \rho_{\rm f}, \tag{6}$$

$$\rho_{a}c_{p,a} = (1 - \phi)\rho_{s}c_{s} + \phi\rho_{f}c_{p,f}. \tag{7}$$

Since the adjacent layers are assumed to be impermeable, the energy equation of Equation 4 is reduced by the advection term to

$$(\rho c_p)_a \frac{\partial T}{\partial t} = k_a \cdot \nabla \cdot (\nabla T).$$
 (8)

Density, heat capacity and dynamic viscosity of water in the aquifer are calculated as a function of temperature and pressure. The material parameter of the solid phase and the adjacent layers are assumed to be constant.

The boundary conditions for pressure and temperature at the outer edge of the aquifer are defined as the initial values for pressure and temperature. This corresponds to the hydrostatic pressure distribution for the pressure and the undisturbed groundwater temperature for the temperature. The same applies to the temperature boundary conditions at the lower and upper surfaces of the adjacent layers, respectively. For accurate simulation of ATES, it is therefore important to ensure that the ATES is modeled to a sufficient size to minimize boundary effects. In the radial direction, this can be estimated by the thermal radius, which is defined as follows:

$$R_{\rm th} = \sqrt{\frac{c_f \cdot V}{c_a \cdot \pi \cdot H}},\tag{9}$$

where  $c_f$  is the volumetric heat capacity of the fluid, V is the total volume of thermal water injected,  $c_a$  is the effective volumetric heat capacity of the aquifer and H is the thickness of the aquifer. The thermal radius indicates how far the thermal plume spreads in a radial direction. However, it should be noted that this estimate does not take into account natural convection, convection due to regional groundwater flow and heat conduction in the vertical direction. Nordell, Snijders, and Stiles (2021) recommends three times the thermal radius as the distance between the hot and cold well to prevent thermal interference. At least one and a half times the thermal radius should be selected for the mapping of a single well.

The adiabatic boundary condition at the inner edge of the neighbouring layers results from the cylindrical implementation of the ATES.

To solve the partial differential equations, the Finite Volume Method (FV) is used for local discretization. The nodes are placed in the center of the control volume. The upwind difference scheme is used as an approximation for the conservation variable. The advantage of this approximation lies in its robustness; it is the only approximation that does not lead to oscillating solutions (Ferziger, Perić, and Street 2020). However, the approximation has a leading truncation error term that is diffusive, i.e. it smoothes the solution. To keep this error term small, the grid must be chosen very finely.

#### 2.2 Model implementation

The model is implemented in Modelica and uses components from the TransiEnt library (Senkel et al. 2021)

and the Clara library (Vojacek et al. 2023). The TIL-Media library available in Clara is used to calculate the temperature- and pressure-dependent properties of pure water. The model can roughly be divided into three levels. The top level represents the overall model of the underground well and can be used for instantiation in larger system levels. In this model, the models of aquifer, adjacent clay layers, well are instantiated and connected. Also the boundaries are set. One level lower the well, the aquifer and the stone layers are described. The energy equation, the continuity equation and the pressure loss model are located in the lowest level.

In Figure 1 the top layer with the models, boundary conditions and connections is shown schematically. The diagram is intended to illustrate that the discretization of the adjacent layers (clay layers) takes place on this level. However, the discretization of the aquifer and the well filter is implemented in the lower levels in order to reduce the number of fluid ports and fluid models. Furthermore, the Figure 1 shows that the *Aquifer* model also has fluid ports in the vertical direction. Thus, modeling of heterogeneous layered aquifers is also possible, as shown in section 3.

The material properties, the geometry of the aquifer and the adjacent layers, the initial conditions are set in a record and can be easily changed in the top level. The mesh for discretization is also set in the record. It is possible to design the discretization in vertical and radial direction very individually. The only restrictions are the same number and size of control volumes in the radial direction for the aquifer and the adjacent layers, as well as the axially symmetrical arrangement of the control volumes of the adjacent layers.

#### 3 Validation

To validate the model, the results are compared with measured values from field experiments at Auburn University in 1981 and their simulation results. The experiment is described in Molz et al. (1983) and the simulation in Buscheck, Doughty, and Tsang (1983).

# 3.1 Experiment and simulation at Auburn University

In the 1970s, Auburn University began a series of field experiments on water storage at temperatures above 35 °C. In the third experiment, injection temperatures were increased on average to 58.5 °C in the first loop and to 81 °C in the second loop to study the effect of buoyancy flow on efficiency (Molz et al. 1983). The geometric, operational and material-related data on the aquifer and the experiment are taken from Buscheck, Doughty, and Tsang (1983). The aquifer under consideration lies at a depth of between 40 and 61 m and is bounded above by a 9 m thick clay layer. Above this is another aquifer. Below the aquifer is a layer consisting of clay, sand and sandstone. The undisturbed groundwater temperature is 20 °C. The

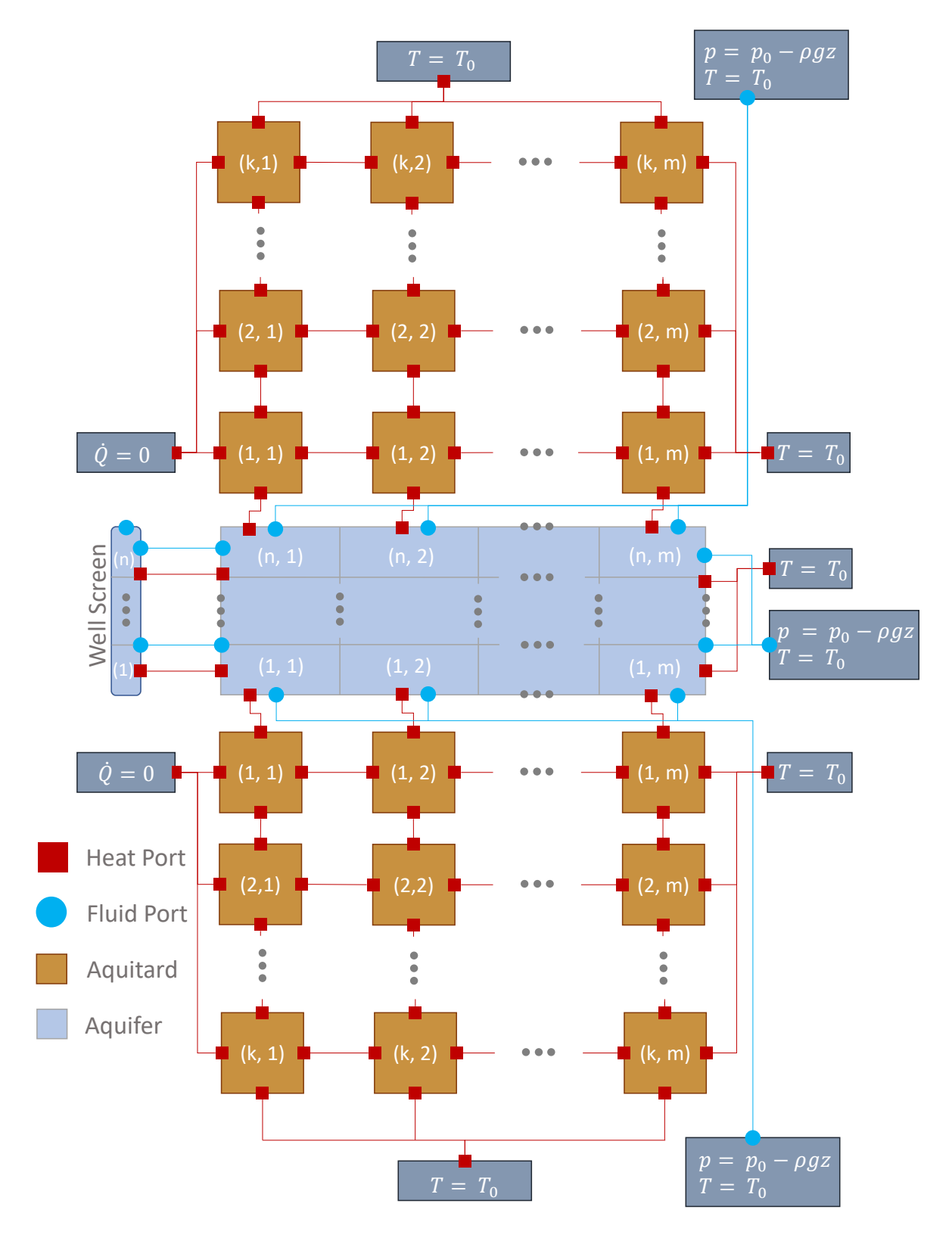


Figure 1. Schematic drawing of connecting the main layers at the top level.

well screen extends across the full thickness of the aquifer and has a radius of 0.1 m. A compilation of the values used in this simulation can be found in Table 1. Although the second cycle is run at significantly higher temperatures, the calculation of the Rayleigh number according to Equation 1 with Ra =  $403 > 4\pi^2 = Ra_{critical}$  shows that buoyancy effects must be taken into account already in the first cycle. Therefore, the validation in this paper focuses on the first cycle.

The operating parameters of the first cycle are listed in the table Table 3. The first period of injection, storage and production lasts just under 87 days. The flow rate and temperature of the water in the injection phase are variable over time in the experiment. For the simulation, Buscheck, Doughty, and Tsang (1983) calculated mean values for injection temperature and volume flow. However, since these values can only be read from a graph, the values were compared to Lopik, Hartog, and Zaadnoordijk (2016).

Table 1. material parameters

Properties	Parameter values
Aquifer properties	
Porosity <sup>1</sup>	0.25
Density of rock <sup>1</sup>	$2600  \mathrm{kg}  \mathrm{m}^{-3}$
Heat capacity of rock <sup>1</sup>	$696.15 \mathrm{Jkg^{-1}K^{-1}}$
Thermal conductivity of aquifer <sup>1</sup>	$2.29\mathrm{W}\mathrm{m}^{-1}\mathrm{K}^{-1}$
Horizontal permeability <sup>1</sup>	$0.63 \times 10^{-10} \mathrm{m}^2$
Vertical permeability <sup>1</sup>	$0.09 \times 10^{-10} \mathrm{m}^2$
Aquitard properties	
Porosity <sup>1</sup>	0.35
Density of rock <sup>1</sup>	$2600 \mathrm{kg}\mathrm{m}^{-3}$
Heat Capacity of rock <sup>1</sup>	$696.15 \mathrm{Jkg^{-1}K^{-1}}$
Thermal conductivity of aquitard <sup>1</sup>	$2.56\mathrm{W}\mathrm{m}^{-1}\mathrm{K}^{-1}$
Fluid properties	1 1
Heat capacity of water	$4186 \mathrm{Jkg^{-1}K^{-1}}$
Thermal conductivity of water	$0.58\mathrm{W}\mathrm{m}^{-1}\mathrm{K}^{-1}$
Geometry	
Aquifer thickness <sup>1</sup>	21 m
Aquitard thickness <sup>1</sup>	9 m
Radius of well screen <sup>1</sup>	0.1 m
Later of a constitution of	
Initial conditions	2000
Initial temperature of aquifer <sup>1</sup>	20°C
pressure of aquifer	5 bar

<sup>&</sup>lt;sup>1</sup> Parameters taken from Buscheck, Doughty, and Tsang (1983).

In Buscheck, Doughty, and Tsang (1983) the field experiment is represented by two models. In the first model the aquifer is assumed to be a homogeneous layer. The second model takes more account of the actual heterogeneity of the aquifer by modelling a three-layer aquifer

**Table 2.** Horizontal permeability and height values for the three layers in heterogeneous model taken from Buscheck, Doughty, and Tsang (1983)

	Thickness in m	<i>Permeability in</i> m <sup>2</sup>
Upper Layer	9.6	$4.6 \times 10^{-10}$
Middle Layer	5	$1.16 \times 10^{-10}$
Lower Layer	6.6	$4.6 \times 10^{-10}$

The vertical to horizontal permeability ratio in each layer is 1:6.

**Table 3.** Operational parameters for the first cycle taken from Buscheck, Doughty, and Tsang (1983).

Phase	Duration in days	Flow rate in m <sup>3</sup> d <sup>-1</sup>	Inj. temperature in °C
Injection	20	760	60
	7	1100	58
	4	600	52
Storage	32	-	-
Production	2	-1684.4	-
	21	-1054.08	-
Rest	26	-	-

where the middle layer has a permeability 2.5 times higher than the two adjacent aquifer layers. The permeabilities and thicknesses of the aquifer layers are given in Table 2. A thickness of 9 m is assumed for the adjacent lower and upper layers and a permeability of  $1\times 10^{-15}\,\mathrm{m}^2$  is assumed for Buscheck, Doughty, and Tsang (1983). For the Modelica simulation, the upper and lower confined layers are assumed to be impermeable to water (aquitard). The temperature distribution in the aquifer and adjacent layers at the end of injection for the homogenous and heterogenous model can be seen in Figure 2.

#### 3.2 Comparison of simulation results

Both models with the homogeneous and heterogenous aquifer are rebuilt in Modelica and the results are compared with the results of the experiment and the two models of Buscheck, Doughty, and Tsang (1983). The comparison is made for the temperature distribution in the aguifer and its adjacent layers at the end of the injection phase and the temperature profile of the water in the well during production phase. The aquifer and its adjacent layers are discretized in volumes with 1 m edge length in vertical direction (except two smaller ones in heterogenous model to rebuild the height of the layers) and 1 m in radial direction until the end of the thermal plume at 40m and then 10 volumes with 3 m. The temperature distribution in the aquifer and its adjacent layers for the homogeneous and heterogenous model at the end of the injection phase is shown in Figure 3a and 3b, respectively. The tilting of the thermal plume due to natural convection can be seen in both figures. In addition, the three layers in the aquifer are clearly visible in the path of the thermal plume in the heterogeneous model. Due to the higher permeability of the middle layer, the largest mass flow is expected there. The temperature distribution in the aquifer and the adjacent layers show a high degree of agreement with the simulations in Figure 2 and the experiment (Buscheck, Doughty, and Tsang 1983, p. 1130). Figure 4 shows the temperature curves of the water during the production phase in the wells for the experiment and all numeric models. The black line shows the measured values of the experiment, the red and green line shows the homogenous and heterogenous model, respectively. The dashed lines are the simulation results of Buscheck, Doughty, and Tsang (1983), the solid lines are the simulation results of this work. The temperature curves of the homogenous model is almost identical to the simulation results of Buscheck. Doughty, and Tsang (1983). The temperature curves of the heterogenous model show a slightly higher temperature in the production well than the simulation results of Buscheck, Doughty, and Tsang (1983). Both Modelica models initially show an increase in well temperature after the start of production. This is due to the different loading temperature of the thermal water during the injection phase and can also be seen in the temperature distribution. This first increase in the well temperature is neither recognizable in the simulation results of Buscheck, Doughty, and Tsang (1983) nor in the measured values from the experiment.

These results show that the Modelica model can not only predict the production well temperature affected by buoyancy, but also model more complex aquifer structures.

# 4 Grid Analysis and 10 Years Simulation

This chapter presents the results of a 10-year simulation of a single well model. It shows that the model can be used as a system component in larger systems and compares the results with and without buoyancy.

For the simulation, the material properties and the geometry of the aquifer are taken from the section 3. A medium sized aquifer with a discharge of  $50\,\mathrm{m}^3\,\mathrm{h}^{-1}$  (Fleuchaus 2020) and a temperature of  $60\,^\circ\mathrm{C}$  is assumed. The calculation of the thermal radius according to Equation 9 results in  $R_{\rm th} = 66\,\mathrm{m}$ . After first impressions of the simulation results, the modeled radius is set to 130 m. To keep the model structure simple, the adjacent layers are represented as 30 m thick aquitards, although there is a wide aquifer above the 9 m thick clay layer. The aquifer is also assumed to be homogeneous. The loading and unloading schedule is kept constant, and the individual phases - injection, storage, production, and resting - each last 91.25 days.

#### 4.1 Grid study

In order to keep the accuracy of the results high and the computational speed as low as possible, a grid study is

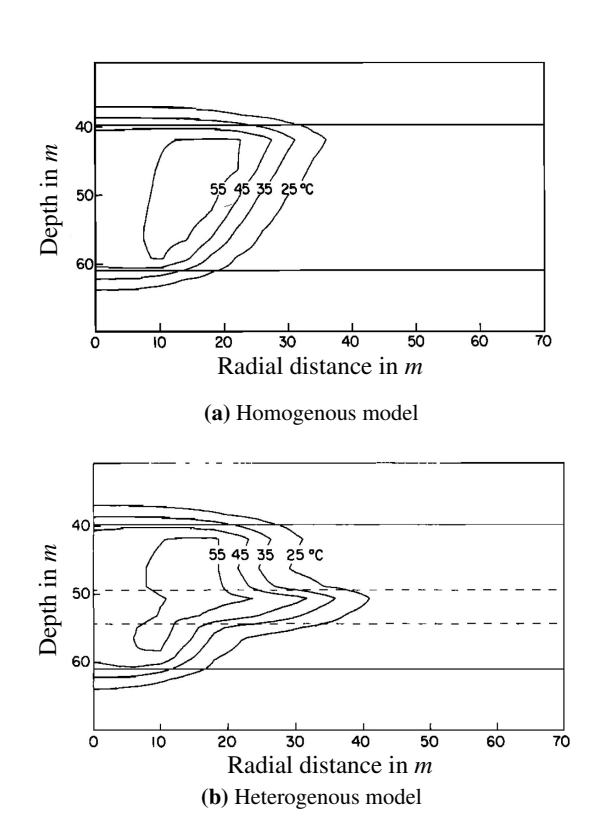


**Figure 2.** Temperature distribution inside the aquifer and its adjacent layers at the end of the injection phase for the homogeneous (a) and heterogeneous (b) model of Buscheck, Doughty, and Tsang (1983).

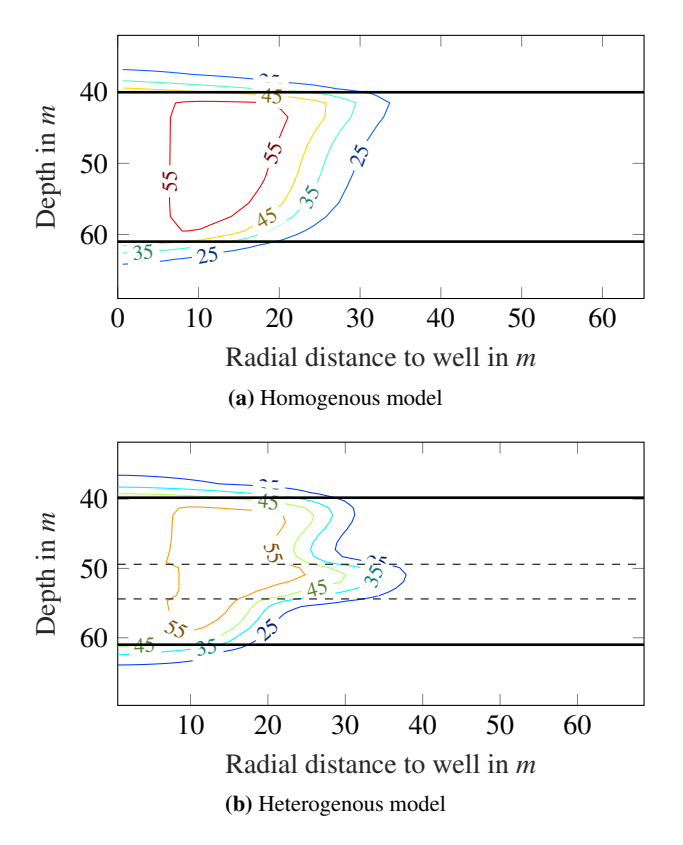


**Figure 3.** Temperature distribution inside the aquifer and its adjacent layers at the end of the injection phase for the homogeneous (a) and heterogenous (b) Modelica model

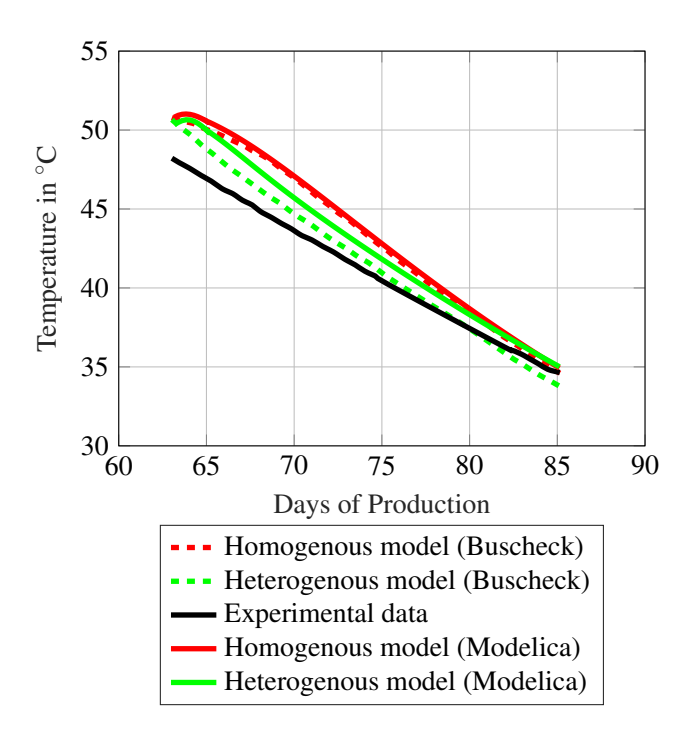


**Figure 4.** Temperature curves of the water during the production phase in the well for the experiment and all numeric models.

essential. For this purpose, a sensitivity analysis is performed in which the grid is changed individually and together in the radial and vertical directions. In addition, the grid structure is changed so that a finer grid structure is chosen in the radius of the thermal plume than outside of it. Inside the plume, the temperature gradients are steeper than outside, depending on the time. This is due to the numerical diffusion by the upwind difference scheme approach in FVM (Ferziger, Perić, and Street 2020).

Table 4 lists the structure of the grids in the sensitivity analysis. A total of nine different grid structures are tested. The first column assigns a number to the individual simulations. The second column lists the number of volumes in the radial direction, vertical direction of the aquifer and vertical direction of the aquitards, in that order. The third column contains the extent of the volumes in meters. If there are vectors in the second and third columns, the columns are assigned to each other. Radially, the discretization is performed from the well; vertically, the discretization is performed from bottom to top for the aquifer and from aquifer to outside for the adjacent layers. The fourth column shows the total number of volume elements. An example for the grid structure is shown in Figure 5.

The first simulation has the finest grid with an edge length of one meter. The subsequent simulations increase the edge length in the radial direction (S2 and S3) and in the vertical direction (S4 and S5). Simulations 6 and 7 combine the changes from simulations 2 and 4 as well as simulations 3 and 5. Simulations 8, 9, 10 and 11 increase the edge lengths outside the thermal plume and in radial direction.

Table 4. Grid Structure Variation

Table 4. Grid Structure Variation						
Number of Simulation	Number of Volumes	Size of Volumes in m	Overall number of volumes			
Firs	t row: Grid i	n radial dire	ction			
Second row	Second row: Grid in vertical direction in Aquifer					
Third row:	Grid in verti	cal direction	in Aquitard			
S1	130 21	1 1	10530			
	30	1				
S2	65 21 30	2 1 1	5265			
<b>S</b> 3	{1,32} 21	{2,4} 1	2673			
S4	30 130 {10,1}	1 1 {2,1}	5330			
S5	15 130 {5,1}	2 1 {4,1}	2860			
S6	{1,7} 65 {10,1} 15	{2,4} 2 {2,1}	2665			
S7	{1,32} {5,1}	2 {2,4} {4,1}	726			
S8	{1,7} {80,10} 21	{2,4} {1,5} 1	7290			
S9	30 {80,5} 21	1 {1,10} 1	3145			
S10	{40,5} 21	{1,2,3,6} {2,10} 1 {1,2,3,6}	1665			
S11	{1,19,5}		925			

21

{1,1,3,3}

{1,2,3,6}

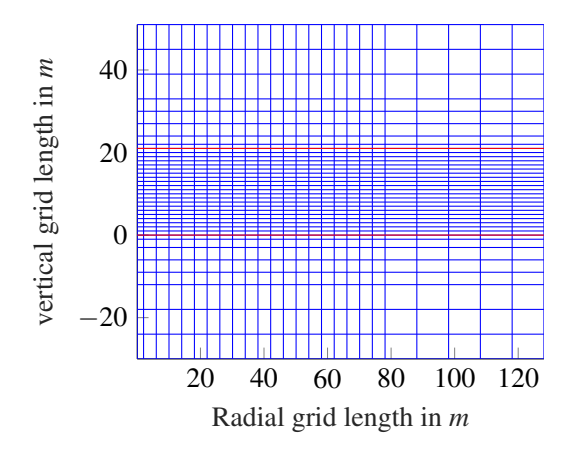
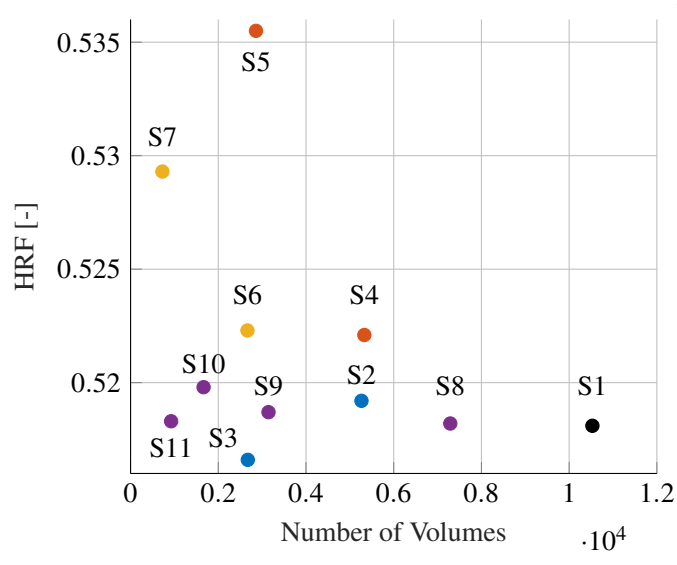


Figure 5. Visualisation of grid structure of simulation S11.



**Figure 6.** Heat Recovery Factor of the individual simulations of grid study after one year operation against the total number of volumes.

The simulations are compared using the Heat Recovery Factor (HRF), which is used as a measure of the efficiency of the ATES after a complete cycle. The HRF is calculated from the ratio of the amount of heat extracted to the amount of heat injected from the thermal water in a cycle:

HRF = 
$$\frac{\int \dot{Q}_{\text{out}} dt}{\int \dot{Q}_{\text{in}} dt} = \frac{\int \dot{m}_{\text{out}} \cdot c_{\text{p}} \cdot (T_{\text{out}} - T_{\text{initial}}) dt}{\int \dot{m}_{\text{in}} \cdot c_{\text{p}} \cdot (T_{\text{in}} - T_{\text{initial}}) dt},$$
 (10)

where  $\dot{Q}$  is the heat flow,  $\dot{m}$  is the mass flow,  $c_p$  is the specific heat capacity, T is the temperature, and  $T_{\rm initial}$  is the temperature of the undisturbed aquifer.

In Figure 6 the HRF of each simulation is plotted against the total number of volumes. The colors of the dots indicate the similarity of the variation. As expected, the coarser the grid structure, the greater the deviation of the HRF from the reference simulation. A coarser grid in the vertical direction in the aquifer has a significantly greater effect on the HRF than in the radial direction. Adjusting the grid outside the thermal plume has the least

effect on the deviation. The number of volumes have a linear impact on the calculation time. By reducing the number of volumes by more than 11 times in simulation S11 compared to the reference simulation, the computation time is also reduced by almost 14 times to 10.2s (Dymola2025x, Advanced.Translation.SparseActivate = true, Solver: DASSL, 1000 intervals, tolerance 0.0001%). Simulation 11 is therefore used for the 10-year simulation.

#### 4.2 10 Years Simulation

The well temperature curve and the HRF of the ATES system are shown in Figure 7a and 7b respectively. In both figures the simulation without buoyancy is compared to the simulation with buoyancy. Comparing the well temperature of the two simulations shows significant differences in the three phases - storage, production and rest. In the storage and rest phases, the well fluid cools significantly faster. This is due to buoyancy and the resulting influx of colder fluid from the lower part of the aquifer. In addition, the lower adjacent layer is less heated than the upper adjacent layer. The production phase is characterized by a steeper decline in well temperature, resulting in a lower temperature at the beginning of the rest phase. This is caused by mixing processes in the well of cold thermal water from the lower part of the aquifer with warmer thermal water from the upper part of the aquifer. This results in a significantly lower heat recovery factor. The evolution of the HRF in Figure 7b of both simulations is similar. After 10 years the ATES has a HRF of more than 1.283% without buoyancy. With buoyancy, the heat recovery drops below 70%. Although the gap to the simulation without buoyancy decreases from over 18 % pt. in the first year to just under 15% pt. in the tenth year, this clearly shows the relevance of considering the buoyancy forces. It can be seen from the two figures that the HRF will increase slightly in the following years.

## 5 Conclusion

The expansion of thermal energy storage is essential for the implementation of the heat transition, and in particular seasonal storage solutions are needed. ATES are a promising technology for seasonal heat storage. With their integration into district heating systems, HT-ATES in particular have become the focus of current research. However, buoyancy effects have to be taken into account in HT-ATES. The author is not aware of any system models that take this effect into account. This paper presents a model for the simulation of HT-ATES systems in Modelica. The model is capable of simulating the thermohydraulic properties of an ATES system with high and low temperature injection. The model has been validated with the results of field tests at Auburn University. The results show that the model is able to predict the temperature distribution in the aquifer and the temperature profiles in the production well with good accuracy. In addition, the model is capable of modeling more complex aquifer models.

A sensitivity analysis of the grid structure has been imple-

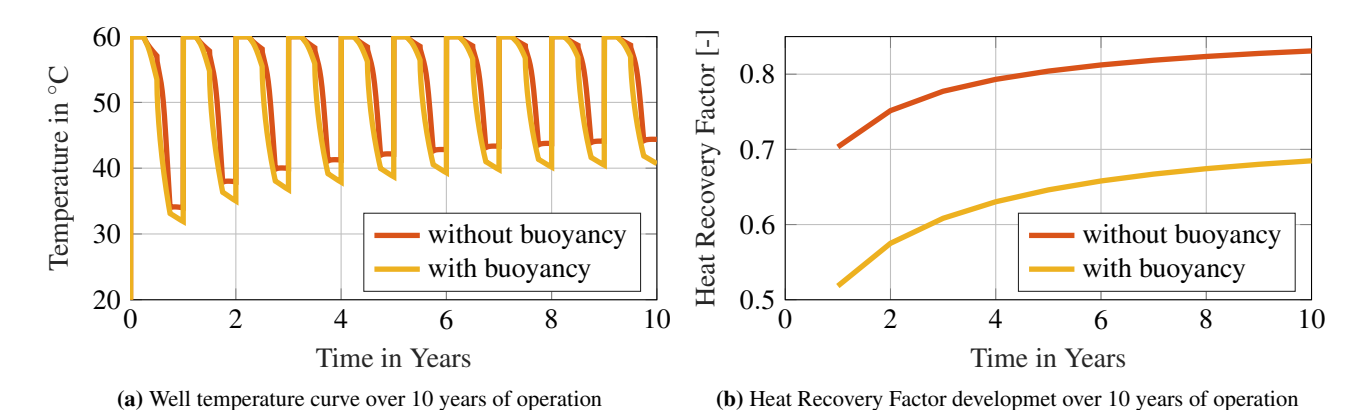


Figure 7. Comparison of well temperature curve and Heat Recovery Factor between simulation with and without buoyancy flow.

mented to reduce computation time in case of acceptable deviations of the heat recovery factors from the reference simulation. The grid analysis shows that outside the thermal plume, the grid structure has less influence on the results. However, the vertical grid structure has a greater influence on the results than the radial grid structure. By adjusting the grid structure, the computation time can be reduced by more than 6 times with an acceptable deviation of the heat recovery factor from the reference simulation. In future work, the optimization of the grid structure in radial and vertical direction could be investigated to achieve further savings in computation time. The relevance of buoyancy effects for the simulation of ATES systems is emphasized by comparing the simulation results with and without buoyancy effects.

# Acknowledgements

The authors greatly acknowledge the funding from the German Federal Ministry for Economic Affairs and Climate Action for the subproject "Planung und Bau eines Aquiferspeichers zur saisonalen Speicherung von Ab- und Überschusswärme" (Design and construction of Aquifer Thermal Energy Storage for seasonal storage of waste and surplus heat, project number: 03EWR007O2) within the project "Reallabore der Energiewende" (Living Labs of the Energy Transition).

#### References

Beernink, Stijn et al. (2024). "Heat losses in ATES systems: The impact of processes, storage geometry and temperature". In: *Geothermics* 117, p. 102889. ISSN: 0375-6505. DOI: https://doi.org/10.1016/j.geothermics.2023.102889. URL: https://www.sciencedirect.com/science/article/pii/S0375650523002444.

Buscheck, Thomas A., Christine Doughty, and Chin Fu Tsang (1983). "Prediction and analysis of a field experiment on a multilayered aquifer thermal energy storage system with strong buoyancy flow". In: *Water Resources Research* 19.5, pp. 1307–1315. ISSN: 00431397. DOI: 10.1029 / WR019i005p01307.

DHI-WASY GmbH (2012). FEFLOW finite element subsurface flow and transport simulation system – Users manual/Reference manual/White papers. v. 6.1. Tech. rep. DHI A/S.

Drijver, Benno, Guido Bakema, and Peter Oerlemans (2019). "State of the art of HT-ATES in The Netherlands". In: *European Geothermal Congress: Proceedings, Den Haag, Netherlands*.

Federal Ministry for Economic Affairs and Climate Action (2024). *Unterirdischer Speicher sorgt für klimafreundliche Wärme*. URL: https://www.energieforschung.de/de/aktuelles/projekteinblicke/2023/unterirdischer-speicher-sorgt-fuer-klimafreundliche-waerme (visited on 2025-02-27).

Ferziger, Joel H., Milovan Perić, and Robert L. Street (2020). "Finite-Volumen-Methoden". In: *Numerische Strömungsmechanik*. Ed. by Joel H. Ferziger, Milovan Perić, and Robert L. Street. Berlin, Heidelberg: Springer Berlin Heidelberg, pp. 91–124. ISBN: 978-3-662-46543-1. DOI: 10.1007/978-3-662-46544-8{\textunderscore}4.

Fleuchaus, Paul (2020). "Global application, performance and risk analysis of Aquifer Thermal Energy Storage (ATES)". PhD thesis. Karlsruhe: Karlsruhe Institute of Technologie. DOI: 10.5445/IR/1000120042. URL: https://scholar.archive.org/work/5ea34jntpnbujilx4574rmapce/access/wayback/https://publikationen.bibliothek.kit.edu/1000120042/77340903.

Fleuchaus, Paul et al. (2021). "Aquiferspeicher in Deutschland". In: *Grundwasser* 26.2, pp. 123–134. ISSN: 1430-483X. DOI: 10.1007/s00767-021-00478-y.

Forschungsinitiative Green Energy Lab (2022). ATES Vienna
- Integrating aquifer thermal energy storage into district
heating networks to achieve complete decarbonisation. URL:
https://greenenergylab.at/projects/ates-vienna/?lang=en
(visited on 2025-02-27).

Gao, H. et al. (2024). "Estimation of Recovery Efficiency in High–Temperature Aquifer Thermal Energy Storage Considering Buoyancy Flow". In: *Water Resources Research* 60.11. ISSN: 1944-7973. DOI: 10.1029/2024WR037491.

Gillner, Markus et al. (2025). "Status of the transient library: Transient simulation of complex integrated energy systems". In: *Modelica Conferences*.

Guelpa, Elisa and Vittorio Verda (2019). "Thermal energy storage in district heating and cooling systems: A review". In: *Applied Energy* 252, p. 113474. ISSN: 03062619. DOI: 10. 1016/j.apenergy.2019.113474.

- Hamburg Insitut (2022). Forschungsvorhaben "Optimierte Integration Thermischer Aquiferspeicher in Fernwäremsysteme" (OptInAquiFer). URL: https://www.hamburg-institut.com/projects/forschungsvorhaben-optimierte-integration-thermischer-aquiferspeicher-in-fernwaermesysteme-optinaquifer/ (visited on 2025-02-27).
- Heldt, Stefan, Christof Beyer, and Sebastian Bauer (2024). "Uncertainty assessment of thermal recovery and subsurface temperature changes induced by high-temperature aquifer thermal energy storage (HT-ATES): a case study". In: *Geothermics* 122, p. 103086.
- Kipp, Kenneth L. (1987). HST3D: A Computer Code for Simulation of Heat and Solute Transport in Thre-Dimensional Ground-Water Flow Systems. U.S. Geological Survey.
- Köhler, Benjamin et al. (2025-02). "Optimierte Integration thermischer Aquiferspeicher in Fernwärmesysteme". In: *3R Rohre*, pp. 84–91.
- Kolditz, O. et al. (2012). "OpenGeoSys: an open-source initiative for numerical simulation of thermo-hydromechanical/chemical (THM/C) processes in porous media".
  In: *Environmental Earth Sciences* 67.2, pp. 589–599. ISSN: 1866-6280. DOI: 10.1007/s12665-012-1546-x.
- Langevin, Christian D. et al. (2017). *Documentation for the MODFLOW 6 Groundwater Flow Model*. Tech. rep. U.S. Geological Survey. DOI: 10.3133/tm6A55.
- Lopik, Jan H van, Niels Hartog, and Willem Jan Zaadnoordijk (2016). "The use of salinity contrast for density difference compensation to improve the thermal recovery efficiency in high-temperature aquifer thermal energy storage systems". In: *Hydrogeology Journal* 24.5, p. 1255.
- Maccarini, Alessandro et al. (2023). "Low-order aquifer thermal energy storage model for geothermal system simulation". In: *Linköping Electronic Conference Proceedings*. Linköping University Electronic Press, pp. 389–396. ISBN: 1650-3686. DOI: 10.3384/ecp204389.
- Molz, F. J. et al. (1983). "Aquifer thermal energy storage: A well doublet experiment at increased temperatures". In: *Water Resources Research* 19.1, pp. 149–160. ISSN: 00431397. DOI: 10.1029/WR019i001p00149.
- Nield, Donald A. and Adrian Bejan (2013). *Convection in Porous Media*. New York, NY: Springer New York. ISBN: 978-1-4614-5540-0. DOI: 10.1007/978-1-4614-5541-7.
- Nordell, Bo, Art Snijders, and Lynn Stiles (2021). "The use of aquifers as thermal energy storage systems". In: *Advances in thermal energy storage systems*. Ed. by Luisa F. Cabeza. Woodhead publishing series in energy. Duxford, United Kingdom and Cambridge, MA: Woodhead Publishing, pp. 111–138. ISBN: 0128198885. DOI: 10.1016/B978-0-12-819885-8.00005-X.
- Push it (2024). *Delft (Netherland) Demo site for Aquifer Thermal Energy Storage (ATES)*. URL: https://www.push-it-thermalstorage.eu/pilots/delft/ (visited on 2025-02-27).
- Schmidt, Thomas (2005). *Aquifer Thermal Energy Storage TR-NAST Two Well Model for TRNSYS*. Tech. rep. Stuttgart: Solites Steinbeis Research Institute for Solar and Sustainable Thermal Energy System.
- Senkel, Anne et al. (2021). "Status of the TransiEnt library: Transient simulation of complex integrated energy systems". In: *Modelica Conferences*, pp. 187–196.
- Umweltbundesamt (2024). Renewable energies in figures. URL: https://www.umweltbundesamt.de/en/topics/climate-energy/renewable-energies/renewable-energies-in-figures (visited on 2025-02-27).

Vojacek, Ales et al. (2023). "Status of the ClaRa Library: detailed transient simulation of complex energy systems". In: *Modelica Conferences*, pp. 617–626.